JOURNAL OF AIRCRAFT
Vol. 49, No. 3, May–June 2012

Multistate Design Approach to Analysis of Twin-Engine Aircraft Performance Robustness

Jeremy S. Agte* and Nicholas K. Borer†
Charles Stark Draper Laboratory, Inc., Cambridge, Massachusetts 02139
and
Olivier de Weck‡
Massachusetts Institute of Technology, Cambridge, Massachusetts 02139

DOI: 10.2514/1.C031338

This article introduces an integrated approach for the early-stage multistate design and analysis of aircraft requiring robust performance across a range of off-nominal system states. It is applied to the case study of an existing twin-engine aircraft, enabled by the development of a multimodal performance model calibrated with flight-test data collected at Edwards Air Force Base Flight Test Center. The methodology includes elements for determining responses in aircraft expected performance and availability to changes in static design variables (geometry), dynamic design variables (control gains), and component failure rates, which are the three driving input categories affecting performance robustness. This is accomplished using Markov chain analysis within the design loop to stochastically model state transitions based on failure rates as well as gain optimization through simulation to ensure controllability at each design point. Results showed unsafe performance in 15% of the King Air geometry-state responses under investigation. Although many occurred in the fully failed state and were expected, five occurred in partially degraded states where the majority of geometries were able to meet performance requirements. Furthermore, this behavior clearly exhibited itself in the resulting design sensitivities, confirming that such an approach allows designers to identify elements that might drive system loss through analysis of performance changes across system states and their respective response to changes in design variables.

Nomenclature

b	=	wing span, ft
$C_{D\delta e}$	=	change in drag coefficient with elevator deflection, 1/rad
$C_{L\delta f}$	=	change in lift coefficient with flap deflection, 1/rad
$C_{l\beta}$	=	change in roll-moment coefficient with sideslip, 1/rad
$C_{l\delta r}$	=	change in roll-moment coefficient with rudder deflection, 1/rad
C_{lp}	=	change in roll-moment coefficient with roll rate, 1/rad
C_{mq}	=	change in pitch-moment coefficient with pitch rate, 1/rad
$C_{m\alpha}$	=	change in pitch-moment coefficient with angle of attack, 1/rad
$C_{n\beta}$	=	change in yaw-moment coefficient with sideslip, 1/rad
C_{nr}	=	change in yaw-moment coefficient with yaw rate, 1/rad
C_{Yr}	=	change in side-force coefficient with yaw rate, 1/rad
$\mathbf{c}$	=	operational parameters
E_A	=	expected system availability
E_G	=	expected performance
G_k	=	performance in state k
Pr	=	transition probability
p_k	=	probability of being in state k
$\mathbf{r}$	=	dynamic design variables
S	=	wing area, ft^2
S_k	=	state k
$\mathbf{x}$	=	static design variables
Γ	=	dihedral, deg
Λ	=	wing sweep, deg
λ	=	taper ratio
λ_i	=	failure rate of ith component

Presented as Paper 2010-2997 at the 51st AIAA/ASME/ASCE/AHS/ASC Structures, Structural Dynamics, and Materials Conference, Orlando, FL, 12–15 April 2010; received 9 December 2010; revision received 30 September 2011; accepted for publication 30 October 2011.

*Draper Laboratory Fellow, 555 Technology Square, MS 27; also Lieutenant Colonel, U.S. Air Force. Senior Member AIAA.

†Systems Design Engineer, 555 Technology Square, MS 27. Senior Member AIAA.

‡Associate Professor, Department of Aeronautics and Astronautics. Associate Fellow AIAA.

I. Introduction

TODAY'S increasingly complex systems are expected to operate in a wide array of environments and conditions. This is particularly true of aircraft, where long design cycles and operational lifetimes virtually guarantee that the system will perform in a variety of scenarios likely not considered during the original development program. In addition, aircraft often experience variation in their design parameters as technologies change throughout their operational life. Each configuration must demonstrate adequate reliability and survivability, where contingency performance metrics of the system must be considered in a variety of degraded modes. These modes can be conveniently modeled within a multistate system, here defined as a system having a finite set of performance levels or performance ranges, each level or range being associated with a distinct vehicle configuration. Although these states may in general include configurations entered by intent or in response to environment, here they are primarily differentiated by distinct levels of failure. The aircraft's performance robustness is determined by the degree to which it consistently achieves expected mission performance across a broad range of operating conditions for a finite set of system states.

To date, the majority of work done with regards to the robustness of multistate systems, especially where formal design and optimization methods have been employed, has focused on three fronts: 1) multistate coherent systems, 2) control design and optimization, and 3) improving component failure rates and redundancy. The first of these deals with systems where a certain coherent structure applies to the various levels of state performance and is the

field where the concept of multistate was first developed in the 1970s [1]. The predictability inherent in these systems allows performance levels to be modeled by a single or set of structure functions and optimized as described in Lisnianski and Levitin [2], but applicability is limited to comparatively simpler systems such as those related to flow (e.g., pumping stations) or data transmission (e.g., circuit boards). In aerospace systems, the complexity of interactions between disciplines and the much larger space of performance metrics limits the usefulness of such methods.

The second area encompasses a large amount of multistate system modeling and design research belonging to the field of control design and control optimization (also referred to as dynamic optimization). The focus on this front is determining the system's state once in operation and effectively controlling it to maximize mission performance. In the case of aircraft, this may include the detection of failure or damage to flight control actuators and using the remaining functional effectors to create compensating forces and moments [3]. Specific cases have developed and tested emergency control laws for partially or completely failed aircraft systems, motivated by the many real-world instances where such control laws may have been helpful [4,5]. Barrett et al. [6] began documenting the extensive development and evaluation of an emergency flight control system for an F-15, continued and completed in Burcham et al. [7,8], using only differential thrust. Results from the 36-flight evaluation showed that such a system can be used to successfully land an aircraft that has suffered from a major flight-control-system failure. A similar endeavor in Ward and Monaco [9] details the successful retrofitting of an F/A-18 with a model-based adaptive control system to respond to states brought about by flight control failure, damage, or adverse environmental conditions. The above instances deal with software-only adaptation to recover from single- or multiple-mode failures by affecting aircraft response through the system's dynamic design or control variables.

The third front turns focus to the system's reliability through failure rate of its components and subelements to improve performance robustness. There are many mature techniques to represent multistate systems for the evaluation of reliability. These include fault trees, reliability block diagrams, and dynamic fault trees [10], some of which have been extended to relatively complex phased-mission analyses [11]. Literature is extensive on the topic, but a good overview can be found in [12,13]. A great deal of successful work has used integrated system modeling with Markov models to determine the system reliability (and system availability) of large, complex systems performing life-critical applications [14,15], or even to model robustness through reconfigurability [16]. Other methods exist, which are more concise in system state specifications, such as stochastic petri nets [17], but generally rely on Markov analyses to solve for state probabilities. The motivation for the research presented in this article originally developed in response to a need for expanding the above type of reliability analysis beyond that involving just component failure rates. Recent work in Dominguez-Garcia et al. [18] began moving in this direction by merging system behavioral analysis with the integrated Markov model generation described in [19], allowing evaluation of performance for multiple system events (e.g., multiple failures and/or sequences of failures) in an F-16. By mapping the effect of system faults into the appropriate performance space, the research acknowledges the link between a system's core static design variables and expected performance in the face of degradation but stops short of manipulating them in a comprehensive manner such that robustness is improved.

Each of the above solutions concentrates predominantly on a single category of the independent variables affecting a system's robustness, namely, on the static design variables, the dynamic design variables, or the component failure rates. Depending on the category into which they fall, most are applied late in the design cycle, after the aircraft's defining characteristics are set. As an improvement to this, the authors apply an integrated approach that includes multiple states of a system earlier in the design process and considers the effects of changes to variables in each of the above three categories. This is tested on a detailed, integrated model of a well-understood problem, that of the design and failure analysis of a C-12C twin-engine turboprop aircraft, which is the military version of the Beechcraft Super King Air 200. This existing aircraft is used as the behavior of its failure modes is understood and should be uncovered by the multistate approach.

It should be noted here that the intention of this approach is not to perform a robustness analysis such as that done under what is often referred to as robust design. In the context of this article, robustness refers to the ability of the aircraft to provide satisfactory performance in the face of changing discrete circumstances, in particular different sequences of component failures. The approach accounts for definable off-nominal aircraft states, arrived at through quantifiable transition rates, and the performance in each of these states is explicitly evaluated. Robust design, on the other hand, typically involves computation of a probabilistic objective function based on probabilistic variation of design variables, a result of uncertainties in analysis capability, manufacturing processes, material properties, etc., to determine the expectation that the real-world aircraft will achieve the desired (typically nominal) performance prescribed in the definition of its requirements. In some cases, probability density functions are also assigned to external parameters to model operational noise. There are many studies that have been done in this area [20–22], and the approach here does not preclude the application of such techniques.

The remainder of this article is organized as follows. Section II describes the main elements and processes of Markov modeling, including the establishment of appropriate measures of merit for characterizing performance robustness. Section III presents the aircraft integrated system model and flight-test data used for its validation. Section IV outlines the general approach as applied to the test case. Section V depicts results of the multistate analysis, including sensitivities of performance metrics to design variables and an analysis of reachability for the worst-performing states.

II. Markov Analysis

A. Behavioral Markov Modeling

Behavioral Markov modeling provides an efficient means of stochastically modeling state transition events and performance outputs that might occur in a large, complex system, without having to perform a full Monte Carlo analysis of the performance space. This is attractive because a Markov chain can explicitly enumerate every unique combination and sequence of possible events regardless of probability. A Monte Carlo analysis, on the other hand, may not find highly improbable event sequences (such as two simultaneous low-probability failures) without a very large number of simulations. This advantage may come at the expense of state-space explosion in the Markov model, which is often controlled by truncating the number of independent events or by aggregating states. Figure 1 shows a generic acyclic Markov-state transition diagram for multiple states of failure without repair or reconfiguration. In this formulation, let p_k be the probability that the system finds itself in any particular state of performance G_k at time t. If one assumes a Markovian process, that is, one in which system states at $t + \delta t$ depend only upon the state at t, all p_k may be determined through the Chapman–Kolmogorov equations [23], knowing the transition probabilities Pr. These transition probabilities, in the case of failures, are typically derived

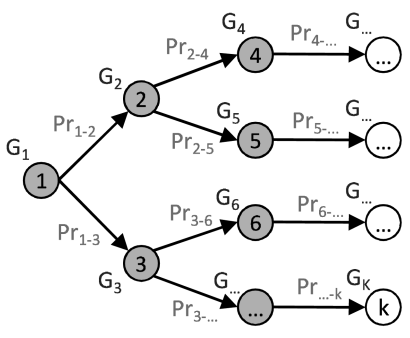

Fig. 1 Markov chain formulation.

from known values of component or element mean time between failure (MTBF). The simplest formulation for the failure rate results in $Pr_{\ldots\to k} = \lambda_i$, where λ_i is the inverse of the MTBF for the ith component.

A simple example, depicted by the Markov formulation in Fig. 2, considers the possible failures of two engines on an aircraft to illustrate the calculation of p_k. For generality, cyclic transitions are allowed via repair rates μ, modeling perhaps a future long-duration air vehicle with onboard diagnostics and possible in-flight repair. State 1 has both engines operating, whereas in state 2 only the starboard engine B is functional and in state 3 only the port engine A is functional. State 4 is the fully failed state in which both engines are nonfunctioning. The λ_i values are the failure rates of A and B while the repair rates feed transition in the upstream direction. Beginning with state 1, for a time period $[t, t+\delta t)$, the probability that the aircraft leaves state 1 is given by

$$P_{1\to} = \lambda_A \delta t + \lambda_B \delta t = (\lambda_A + \lambda_B)\delta t \tag{1}$$

Subsequently, it follows from the Chapman–Kolmogorov equations that the probability of being in state 1 at time $t+\delta t$ is determined from

$$p_1(t+\delta t) = p_1(1 - (\lambda_A + \lambda_B)\delta t) + p_2\mu_A\delta t + p_3\mu_B\delta t \tag{2}$$

which, after extending to the other three states and differentiating at the limit as δt approaches zero, provides the system of first-order linear differential equations:

$$\frac{\mathrm{d}\mathbf{p}(t)}{\mathrm{d}t} = A\mathbf{p}(t) \tag{3}$$

where A is the matrix shown in Eq. (4):

$$A = \begin{bmatrix} -(\lambda_A+\lambda_B) & \mu_A & \mu_B & 0 \\ \lambda_A & -(\mu_A+\lambda_B) & 0 & \mu_B \\ \lambda_B & 0 & -(\mu_B+\lambda_A) & \mu_A \\ 0 & \lambda_B & \lambda_A & -(\mu_B+\mu_A) \end{bmatrix} \tag{4}$$

Whereas 20 years ago the solution to Eq. (3) required careful formulation regarding computational efficiency, today many commercial solvers exist capable of rapidly executing it for hundreds or even thousands of states.

In practice, combining the Markov model construction of more complex architectures with an integrated system model allows the user to enumerate the dependency structure of the individual components. This capability ensures that dependent failures or cascading effects are adequately represented in the reliability estimates, which are not typically captured through traditional reliability estimation techniques [24].

B. System Availability and Expected Performance

The behavioral Markov approach enables far more than system reliability analysis. Properly generalized, it allows for the rigorous enumeration of performance associated with any probabilistic sequence of discrete events. Although the user must understand the impact of these singular events, they only need to model the effects on the initiating element. The integrated behavioral model then captures the cascading effects through the complete system. The Markov model will generate all possible event sequences (to a user-specified number of random events), and the behavioral model will capture the performance and stability as it cascades through the integrated system for each particular event sequence.

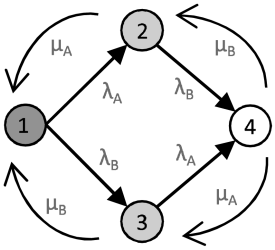

Fig. 2 Two-engine failure scenario.

Following the nomenclature of Fig. 1, if the performance levels G_k can be determined, it is possible to determine the system's overall availability E_A and expected performance E_G according to Eqs. (5) and (6), taken from Levitin and Lisnianski [25]. Here, T represents a designated period of time, often divided into M intervals of T_M, where each interval may have its own acceptable minimum performance level W_M. $Q(W_M)$ is the summed probabilities of those states that have achieved at least W_M in time interval T_M:

$$E_A = \sum_{m=1}^{M} Q(W_M)\frac{T_M}{T} \quad \text{where } Q(W_M) = \sum_{G_k \geq W_M} p_k \tag{5}$$

$$E_G = \sum_{k=1}^{K} p_k G_k \tag{6}$$

Although each of these metrics is useful in its own right, they are far more powerful when combined with system sensitivity analysis. Namely, it is desirable to know how these quantities change as system variables are modified. This approach has been used in the past for system reliability analysis [14,26], using only the component failure rates. In these cases, the absolute system reliability was of less concern than identifying those elements that drive the system loss probability. These elements were discovered through sensitivity analysis, solving Eq. (5) for $i = k$ number of cases, where each case modified the failure rate of the ith component. The components that drive system loss are those that exhibit the largest sensitivity, or change in E_A, given a change in λ_i. Using the example from Fig. 2, assuming a single, fixed time period (i.e., $T_M = T$) and that state 4 is the only one in which the aircraft cannot achieve W_M (a positive rate of climb), this sensitivity appears as

$$\frac{\mathrm{d}E_A(\boldsymbol{\lambda}, \boldsymbol{\mu})}{\mathrm{d}\boldsymbol{\lambda}} = \sum_{k=1}^{3} \frac{\mathrm{d}p_k(\boldsymbol{\lambda}, \boldsymbol{\mu})}{\mathrm{d}\boldsymbol{\lambda}} \tag{7}$$

which can, of course, also be shown for the repair rates $\boldsymbol{\mu}$. The sensitivity here is not necessarily used for direct optimization; it is elementary to know that reducing a component failure rate will (generally) increase reliability. Rather, it is used to point the system designers to the portion of the system architecture that has the greatest effect on reliability. The remedy may lie with finding a higher-reliability component, introducing redundancy, changing mission parameters, or a host of other solutions.

System sensitivity analysis can be extended to include effects of static, or geometric, variables on expected performance E_G. In this way, it is possible not only to observe sensitivity of the expected performance to component failure rates but also traditional aircraft design variables $\mathbf{x}$ (wing span, wing area, engine placement, etc.) and operational parameters $\mathbf{c}$ (cruise altitude, cruise speed, etc.). Following the same assumption on time as Eq. (7), this takes the form

$$\frac{\mathrm{d}E_G(\boldsymbol{\lambda}, \boldsymbol{\mu}, \mathbf{x}, \mathbf{c})}{\mathrm{d}\mathbf{x}} = \sum_{k=1}^{K} p_k(\boldsymbol{\lambda}, \boldsymbol{\mu}) \frac{\mathrm{d}G_k(\mathbf{x}, \mathbf{c})}{\mathrm{d}\mathbf{x}} \tag{8}$$

for sensitivity with respect to design variables $\mathbf{x}$. Note that, by way of the inequality in the summation for Q in Eq. (5), expected availability becomes a function of $\mathbf{x}$ and $\mathbf{c}$ as well, although not necessarily a continuous one.

The individual Markov-state probabilities p_k in Eqs. (6) and (8) act as weights to a weighted performance equation. Hence, for short missions, where there is little chance for the system to enter any but the nominal state, expected performance sensitivity will look much like a standard design sensitivity analysis. However, as system lifetime or mission duration increases, the probabilities of the off-

nominal Markov states increase and sensitivities may change dramatically. Consider, for example, the recent solicitation for proposals from the Defense Advanced Research Projects Agency for an ultra long-endurance UAV with an on-station time of five years [27]. In this case, expected performance sensitivity is a promising metric for identifying those system parameters that have the greatest effect on both nominal and off-nominal system performance, and this analysis may be critical for mission success.

III. Aircraft Integrated System Model

The expected performance and availability analysis outlined in the previous section represents a significant departure from traditional analyses encountered during aircraft conceptual design. It hypothesizes the existence of cross-sensitivities between what may be considered traditional aircraft design variables affecting performance (such as wing area, wing span, tail height, etc.) and traditional parameters that affect reliability (such as component failure rates). Hence, a compelling case can be made for this methodology by demonstrating that such cross-sensitivities (e.g.,, the effect of tail height on system reliability) exist and can be captured at the conceptual level. As such, a series of integrated low- to medium-fidelity analyses, representative of the toolset used by an aircraft designer during system conceptual design, was constructed to demonstrate the existence of these sensitivities. This aircraft integrated system model was calibrated to flight-test data from a well-characterized twin-engine aircraft, which was then perturbed in a situation similar to that of a design engineer seeking first-order sensitivities for various design variables and component failure rates on the metrics presented in the previous section (expected performance and expected availability).

The early-phase aircraft system design model developed for this demonstration is divided into an aspect-oriented hierarchy with subdisciplines of mass properties, aerodynamic forces and moments, propulsion, and performance. Figure 3 shows a simplified depiction of the design model information flow. All geometry is entered as basic aircraft design variables such as aspect ratio, taper ratio, wing sweep, fuselage height and width, engine location, etc., which are used to calculate mass and inertias for the aircraft's various components. These geometric parameters are also passed to a preprocessor for input to a vortex lattice code as geometric coordinates for discretized lifting surface panels. A few of the geometric parameters are handled directly by a flight simulator executable in the performance module, such as the location of the fuel tanks, included so that the inertial effects of fuel burn may be directly accounted for during run time. The dotted lines in the feedback from performance to mass properties and aerodynamic forces and moments indicate the potential effect of engine size and weight on these two disciplines. They are not linked in the current model because the analysis in this study assumes a specific engine that does not vary in maximum thrust or size.

A. Disciplines

The mass properties discipline computes various component weights using empirically based equations from Brandt et al. [28] and Raymer [29]. Inertias are then calculated for each of these components by discretizing them into smaller divisions, computing the divisional centers of gravity, and summing the discretized inertias to get I_{xx}, I_{yy}, I_{zz}, and I_{xz} for the wing, tail, fuselage, etc. The remaining products of inertia I_{xy} and I_{yz} are not considered due to the aircraft's symmetry of mass and geometry about these axes. Each component value is passed to the aerodynamic forces and moments module, where total vehicle inertias are computed through the parallel axis theorem and used to help determine the aircraft's response characteristics. All of the code in the mass properties discipline is written in MATLAB®.

A vortex lattice solver is used in the aerodynamic forces and moments discipline. This is the publicly available GNU-licensed Athena Vortex Lattice (AVL), which employs an extended vortex lattice model for lifting surfaces and a slender body model for fuselages and nacelles [30]. AVL has been widely used in many aerodynamic analysis applications, including the calculation of stability and control derivatives for flight simulation in [31,32] as well as stability and performance analysis in [33]. It represents lifting surfaces as single-layer vortex sheets that are discretized into horseshoe vortex filaments, where the velocities induced at a specific control point are calculated by the Biot–Savart law. Pressure differentials and circulation between the upper and lower surfaces of the wing, tail, etc., are connected to the vortex strengths and total forces are obtained by integration of the pressure differentials. The forces are computed not only on the bound vortex legs but on parts of trailing vortex legs that lie on physical surfaces, allowing better evaluation of moments due to sideslip. Control derivatives are calculated through specification of a hinge-line location in coordination with surface size and deflection. Fuselages and

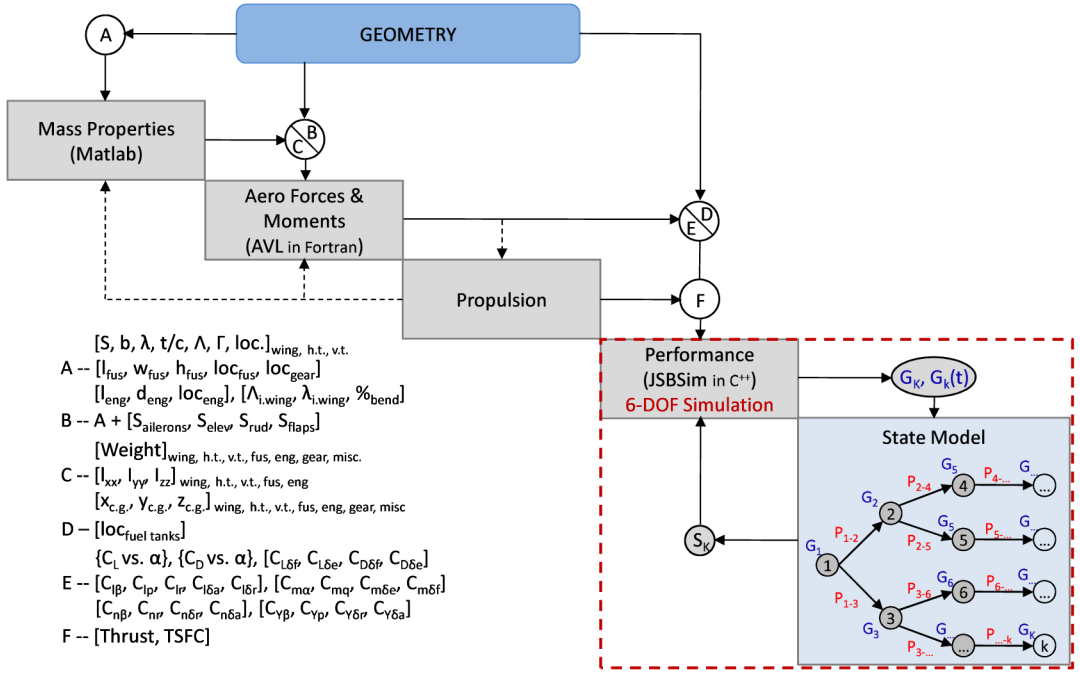

Fig. 3 Multistate aircraft design model data flow.

Table 1 Maximum observed angle ranges

Run case	Observed α range, deg	Observed β range, deg	Observed δ_r range, deg	Observed δ_e range, deg
State 4, geometry 4[a]	6 to 7	−4 to −2	−12 to 17	−12 to 14
State 4, geometry 10	5 to 7	−3 to −2	−12 to 16	−12 to 14
State 4, geometry 12	−18 to 19	−13 to 9	−13 to 13	−14 to 14
State 4, geometry 15	5 to 6	−3 to −5	−13 to 17	−12 to 14

[a]See Sec. V for details on these run-case configurations. The aileron is failed in state 4; thus, δ_a is not reported.

nacelles are represented as source-doublet filaments, where the resulting force and moment calculations are consistent with slender body theory. Standard assumptions for vortex lattice apply, including that of quasi-steady flow (unsteady vorticity shedding is neglected) and small angle approximations. Quasi-steady wake shedding of the fuselage is modeled. The authors acknowledge that certain interference effects and nonlinearities not captured by AVL may affect real world aircraft performance to a larger degree than represented in the analysis, but for purposes of early-phase design evaluation such assumptions are typically standard and necessary.

Regarding the small angle approximations, 99.5% of the run cases reported on in Sec. V do not exhibit angles of attack (AOAs) or sideslip above ± 15 deg, and the vast majority of these are below ± 10 deg. Table 1 shows the four worst-performing run cases and their maximum observed angle ranges, including control-surface deflection angles. Even in the single worst-performing run case (state 4, geometry 12), all angles remain below ± 20 deg, which may be considered on the limit of marginal accuracy for this stage of design.

AVL is written in Fortran and takes as input the aircraft geometry coordinates (which, in this case, have been processed from the aircraft geometric design variables) and specified mass properties. Output data are all of the aircraft control derivatives passed to the performance module shown in Fig. 3. This is also where the aircraft's drag polar is calculated, providing both C_L and C_D as a function of AOA. Lift and drag characteristics for various flap configurations (leading or trailing edge) may be computed as a function of AOA as well. These are determined for any aircraft geometry coming out of the aerodynamics module and then used in the performance simulation to model various in-flight configuration changes.

Thrust and specific fuel consumption are calculated in the propulsion discipline, which at this time is a lookup table for each of these values based on flight speed and altitude. In the future, this will be updated to consider different size engines during the design cycle such that engine weight and nacelle drag may also be treated as variables. Although the aerodynamic effects of thrust on lifting surfaces are not accounted for at this time, other engine effects such as throttle lag, p factor, and location specific forces and moments (e.g.,, windmilling drag) are included in the analysis.

The heart of the design model is an open-source six-degrees-of-freedom flight simulator called JSBSim [34], modified to run in batch mode as an *S* function in MATLAB's Simulink®. The development of JSBSim began over a decade ago with Berndt [34], and over the years has grown into a major project involving dozens of engineers. It is very powerful as a means of evaluating aircraft flight dynamics and includes the means for fully configuring the flight control system, propulsion, aerodynamics, and landing gear of any general aircraft. This is typically done through a front-end extensible markup language (XML) input file, where the aircraft's characteristic parameters are read in once at the onset of the simulation and then control inputs are treated as dynamic properties updated several times per second during run time. Mills [35] began work on the basic implementation of the *S* function over a year ago and the authors continued its further development for the work presented in this article, including modifications to the flight simulation engine itself. The resulting updates to the code (C++) enable the effects of nearly all aircraft design variables to be treated as dynamic properties in the same way as control inputs, such that they can be varied as a functions of time during the execution of the flight model in Simulink. This makes possible the rapid evaluation of a wide range of aircraft performance parameters for a nearly limitless number of aircraft configurations, including simulation of failure states, e.g., loss of actuators and engine failures.

B. Aircraft Model

To demonstrate the multistate design problem, the analysis begins with the baseline configuration of a Beechcraft Super King Air Model 200, as shown in Fig. 4. This aircraft was chosen because its behavior is well understood and there is ample geometry data which is publicly available [36,37]. Additionally, the first author has numerous flight hours testing the C-12C, which is the Air Force modified version of the Super King Air to which this particular computational model was calibrated. The aircraft is powered by two Pratt and Whitney PT6A-41 turboprop engines, each rated at 850 hp (sea level), and is equipped with a rudder-boosted yaw damper system.

Care was taken to ensure that results from the vortex lattice analysis and from flight simulation were representative of the real-world aircraft. Thus, comparisons were made to results from a flight test validated model derived from an in-flight performance evaluation of the Beech C-12C performed at Edwards Air Force Base in 2001 [38], and raw flight-test data from an extensive program to estimate the C-12C aerodynamic stability and control derivatives at Edwards Air Force Base in March of 2010 [39]. The results from the 2001 aerodynamic model shown in Fig. 5 come from the Air Force

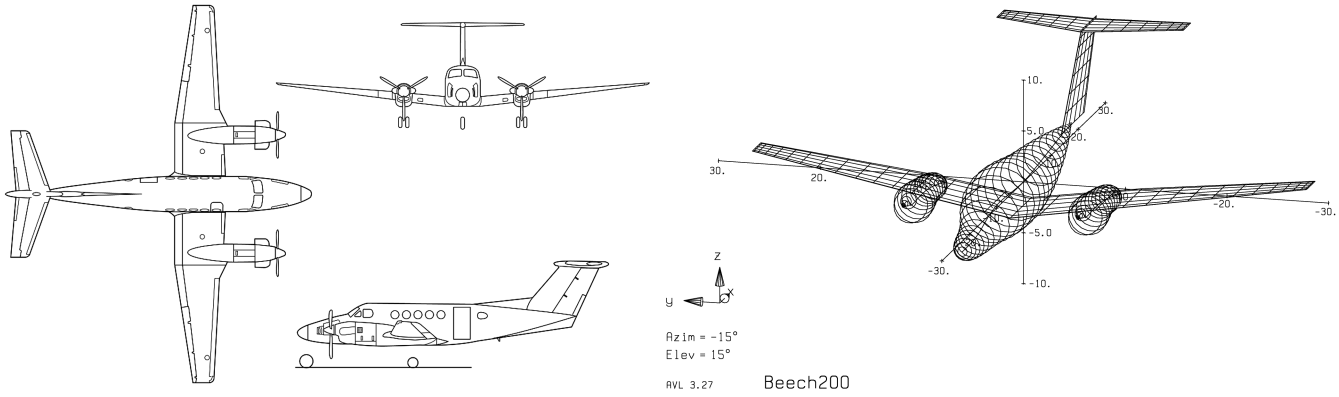

a) 3-view (public domain) **b) AVL representation**

Fig. 4 Beech C-12C (Super King Air Model 200).

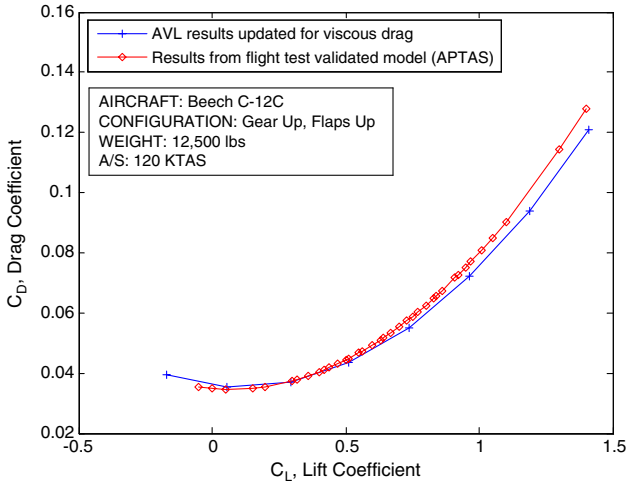

Fig. 5 Drag polar comparison (flight-test data from October 2001).

Flight Test Center Post Test Analysis System (raw data results were not available) and exhibit satisfactory comparison to the AVL data, which were updated for viscous drag through the drag component buildup method.

Data from the more recent testing in 2010 were compared to the stability and control characteristics of the integrated model. In general, the existing precalibrated model arising from the analyses depicted in Fig. 3 was quite accurate and only small adjustments (less than 5% from baseline) were made to the mass estimation routines and control surface geometries to reach the demonstrated results for AOA and sideslip shown in Figs. 6 and 7. The data depicted in Fig. 6 show excellent matching between the computed and flight-test AOA response to an elevator doublet, with a root-mean-square error (RMSE) of less than 0.4 deg. In the yaw axis, shown in Fig. 7, results are satisfactory in that both response frequencies are the same, although the computed model shows more damping than the actual aircraft response, resulting in a higher RMSE of 1.81 deg. This does not significantly affect the impact of this study's results for two reasons. First, although the flight-test response implies a less-damped Dutch roll mode than the simulation, the simulation is nonetheless very successful in capturing the performance degradation due to the King Air's Dutch roll mode, as will be shown in Sec. V. Second, a more comprehensive estimate of the aircraft's yaw–roll interaction is $|C_{n\beta}/C_{l\beta}|$. As described in Sec. V, the aircraft model predicts a $|C_{n\beta}/C_{l\beta}|$ of 0.38, whereas that derived from the flight test is 0.35 and comes from data across several flights. Both $|C_{n\beta}/C_{l\beta}|$ values are in close agreement and border the region typically indicative of poorly damped Dutch roll.

Finally, Table 2 shows a sampling of the baseline aircraft stability and control derivatives for both longitudinal and lateral–directional axes.

IV. Approach

The next step is to examine the relationship between the aircraft's static design variables and its performance output for differing aircraft states. This may be used to evaluate the expected performance and availability of the system across various time periods and subject to changes in component or element MTBF. Here, we establish that such a relationship exists and can be useful for more detailed performance evaluation and tradespace exploration for robust, long-endurance system concepts.

A. State Definition

The number of failure cases and all of their permutations can be quite large in any particular multistate analysis. In this initial examination, we chose to limit failures to those most directly affecting performance and dynamics, specifically failure of the rudder, ailerons, and/or a single engine. These correspond to the failure rates λ_R, λ_A, and λ_E, respectively. Failure rates were set at values of 2×10^{-6} failures per hour for the rudder and ailerons and 8×10^{-6} failures per hour for the engine, which was then doubled because only the possibility of losing one engine was considered. Engine failure rates for the Pratt & Whitney PT-6 come from [40], and a more detailed discussion of the flight control failure rates is given in Appendix A.

If sequence dependence is ignored, this leaves only eight system configurations to consider, as depicted in the aggregated Markov model shown in Fig. 8. This model appears somewhat different from that shown in Fig. 1 because several of the downstream states can now be reached from multiple upstream states due to the aggregation. The ODE solution of the model to determine each state probability p_k, however, is performed in the same manner. The states in the aggregated Markov model are shown in Table 3.

Two time periods were used for the analysis of the Markov model and calculation of state probabilities p_k. The first was a typical

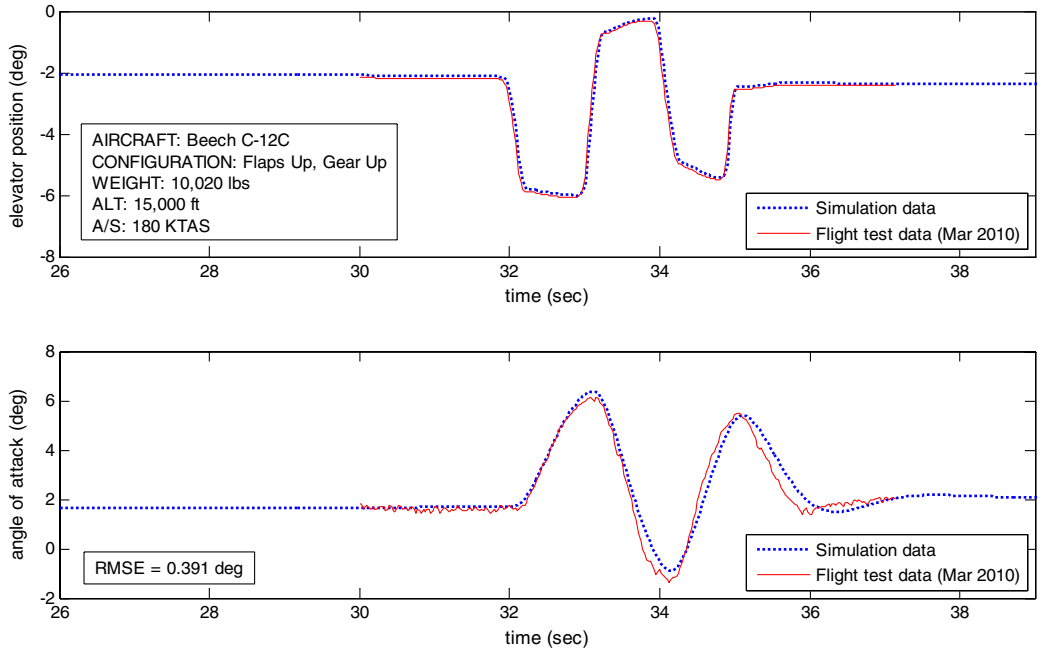

Fig. 6 Comparison of AOA response.

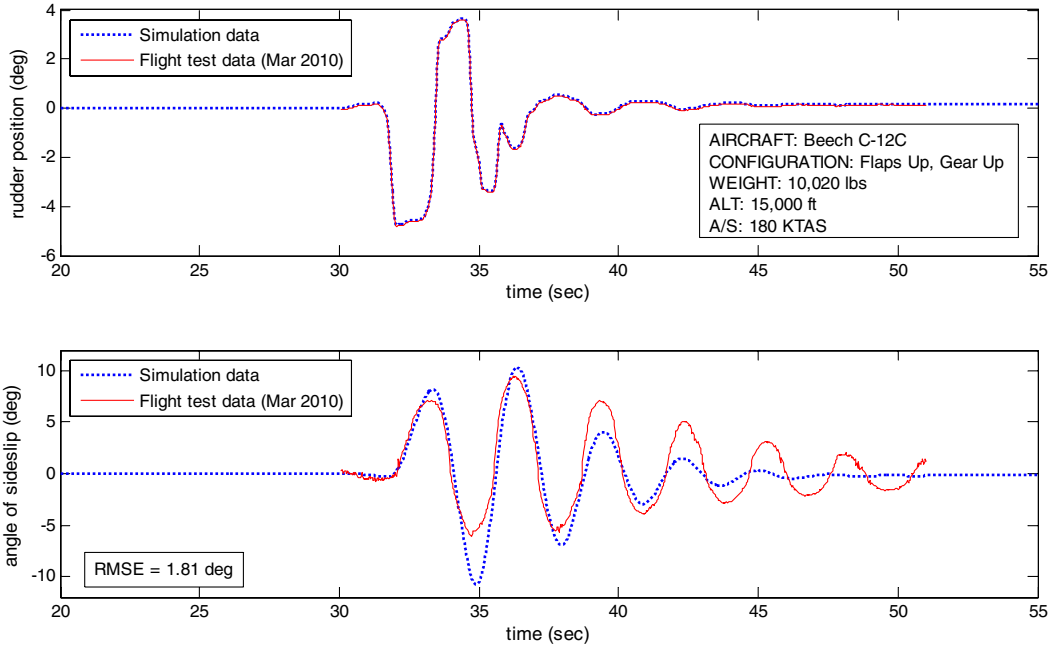

Fig. 7 Comparison of angle-of-sideslip response.

mission duration of 8 h and the second was a 20,000 h time period providing an indication of problem areas that might manifest themselves over the system lifetime. Results for both time periods are provided in Sec. V.

B. Aircraft Performance Metrics

The performance function of interest is cast as expected specific excess power P_s in a climbing turn, which must be evaluated for the nominal condition and each of the failure states to compute Eqs. (5) and (6). P_s is computed from the flight simulation code using the outputs $\mathrm{d}h/\mathrm{d}t$, $\mathrm{d}V/\mathrm{d}t$, and V in the equation $P_s = \mathrm{d}h/\mathrm{d}t + (V/g)(\mathrm{d}V/\mathrm{d}t)$. The expected performance and availability equations resulting from this formulation are given in Eqs. (9) and (10):

$$E_G(P_s(\mathbf{x}),\boldsymbol{\lambda}) = \sum_{k=1}^{8} p_k(\boldsymbol{\lambda}) P_s(\mathbf{x})_k = \sum_{k=1}^{8} p_k(\boldsymbol{\lambda}) \left[\dot{h}(\mathbf{x}) + \frac{V(\mathbf{x})}{g}\dot{V}(\mathbf{x})\right]_{\mathrm{avg},k} \tag{9}$$

$$E_A(P_s(\mathbf{x}),\boldsymbol{\lambda}) = \sum_{[\dot{h}(\mathbf{x})+\frac{V(\mathbf{x})}{g}\dot{V}(\mathbf{x})]_{\mathrm{avg},k} \geq W_M} p_k(\boldsymbol{\lambda}) \tag{10}$$

Here, h is altitude, V is velocity, g is the gravity constant, and the "avg" subscript indicates the values are averaged over the last 20 s of the simulation, allowing the aircraft a chance to stabilize before the performance metric is computed. W_M is defined as 200 ft/ min for a minimum safe rate of climb, allowing calculation of Eq. (10), and bank angle must be maintained within ±5 deg to be in the safe region for calculation of $E_A(\phi(\mathbf{x}),\boldsymbol{\lambda})$. Total availability then becomes

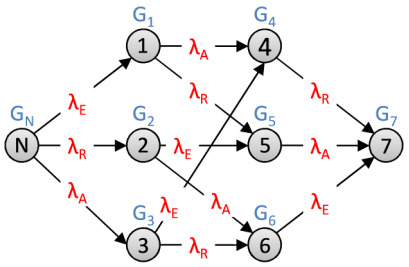

Fig. 8 Problem specific Markov formulation.

$$E_A(P_s(\mathbf{x}) \cap \phi(\mathbf{x}),\boldsymbol{\lambda}) = \sum_{P_s(\mathbf{x})\geq 200 \text{ fpm } \& \ \phi_{\mathrm{dev}}(\mathbf{x})\leq \pm 5^\circ} P_K^s(\boldsymbol{\lambda}) \tag{11}$$

Each simulation was run for a period of 60 s (accelerated in batch mode), beginning from a full-throttle, constant-velocity climbing turn at 30 deg of positive bank (to the right). Initial conditions were set at an altitude of 5000 ft and a velocity of 140 kt, which is close to the best speed for a cruise climb in the Beech 200. Engine failure was

Table 3 Aircraft states

State	Rudder	Aileron	Left engine	Turn control
Nominal (N)	G[a]	G	G	Ailerons/rudder
State 1	G	G	F[a]	Ailerons/rudder
State 2	F	G	G	Ailerons
State 3	G	F	G	Rudder
State 4	G	F	F	Rudder
State 5	F	G	F	Ailerons
State 6	F	F	G	Differential thrust
State 7	F	F	F	n/a

[a]G denotes good; F denotes failed neutral (actuators) or failed off (engine).

Table 2 Baseline stability and control derivative values

Long.	C_{L_α}	$C_{L_{\alpha=0}}$	C_{m_α}	$C_{m_{\alpha=0}}$	C_{m_q}	$C_{m_{\delta_e}}$
	5.27/rad	0.296	−0.541/rad	0.134	−33.9/rad	−0.0422/rad
Lat.–dir	C_{n_β}	C_{l_β}	C_{l_p}	$C_{l_{\delta_a}}$	C_{n_r}	$C_{n_{\delta_r}}$
	0.0454/rad	−0.119/rad	−0.559/rad	−0.00457/rad	−0.132/rad	0.00138/rad

Table 4 Aircraft geometry perturbations

Design variable:	Low Value	Baseline	High Value
Wing area	272.7 ft^2	303 ft^2	333.3 ft^2
Wing span	49.05 ft	54 ft	59.95 ft
Horizontal tail area	65.7 ft^2	73 ft^2	80.3 ft^2
Horizontal tail span	16.51 ft	18.3 ft	20.17 ft
Vertical tail area	105.12 ft^2	116.8 ft^2	128.48 ft^2
Vertical tail height	7.5 ft	8.33 ft	9.16 ft
Spanwise engine location	7.72 ft	8.58 ft	9.44 ft
Aileron chord[a]	15.3%	23%	30.7%
Elevator chord[a]	23%	30%	37.0%
Rudder chord[a]	17.5%	25%	32.5%
Wing sweep	0 deg	4 deg	15 deg

[a]The design variables to which the +10% perturbations were applied are the distances between the leading edge of the lifting surface and the leading edge of the detecting control surface. This dimension facilitates input to the vortex lattice code but is meaningless to the reader without the chord length.

modeled by cutting the throttle to zero after 10 s and control failures disallowed the use of the control surface throughout the simulation, assuming that it was stuck in the neutral position. In the case of engine failure, the model accounts for additional drag effects of the windmilling engine.

Rather than perform the full reoptimization of an existing aircraft, at this stage the interest was in identifying those elements that might drive system loss probability through sensitivity analysis. Therefore, a subset of aircraft geometry variables were selected and their values perturbed by $\pm 10\%$, with the exception of wing sweep, which was varied from 0 to 15 deg. These variables and their values are given in Table 4. Baseline values correspond to those of the aircraft in Fig. 4. Note that the values for the deflecting control surfaces are displayed to the reader as percentages of wing, horizontal tail, or vertical tail chord, for ease of interpretation, although these are not the actual design variables (see footnote on Table 4).

C. State and Geometry-Specific Gain Optimization

Proportional–integral–derivative controllers with a lead–lag compensator were used to maintain airspeed (elevator channel), bank (channel dependent on failure state), and yaw (rudder or throttle channel according to state), according to the block diagram in Fig. 9.

To ensure the aircraft maintained the best possible control while achieving the bank and climb requirements, gains **r** for each of these controllers were tuned by first using the Ziegler–Nichols (Z–N) method [41] to determine a feasible starting point and then by fine tuning with an interior-point constrained optimization algorithm according to the optimization formulation given in Eq. (12), shown for the bank angle task:

$$\begin{aligned} &\text{given state } S_k, \qquad \text{geometry } \mathbf{x} \\ &\text{minimize } J(\mathbf{r}) = \frac{\sum(\phi - \phi_{\text{setpoint}})^2}{t/\Delta t} \\ &\mathbf{r} = [R_p, R_i, R_d, R_{LL1}, R_{LL2}, R_{LL3}, R_{LL4}] \\ &\quad \text{s.t. } r_{i,\text{LB}} \le r_i \le r_{i,\text{UB}}, \qquad i = 1, 2, \ldots, n \end{aligned} \tag{12}$$

The lead–lag compensator was used when necessary, constructed as

$$\frac{R_{LL1}s + R_{LL2}}{R_{LL3}s + R_{LL4}} \tag{13}$$

such that when the coefficients are $[R_{LL1} = 0, R_{LL3} = 1, R_{LL2} = R_{LL4}]$, it becomes strictly a lag compensator and when all coefficients are zero, the compensator is not in use.

The above tuning and optimization procedure proved very effective and often the Z–N results were more than sufficient to control a wide range of states S_k and geometries **x** to within negligible deviations. This was especially true in the longitudinal axis for the control of airspeed. For the cases where more refinement was required in the roll axis, the optimization in Eq. (12) was performed from 10 random starting points within the bounds on **r** determined from the Z–N results to better search the nonlinear design space. If bounds were reached, they were readjusted and the process reinitialized. The worst-performing cases at the end of the procedure were then analyzed according to their reachability characteristics as reported in Sec. V and Appendix B.

V. Results

Each geometry in Table 4 was run for each Markov state, including one baseline geometry plus 11 low values and 11 high values for a total of 23 geometries. This resulted in 184 simulation runs when applied to the eight Markov states. Total computational time, not including gain optimization, was under two minutes when split in parallel across eight processing threads on a desktop with an Intel quad-core i7 2.8 GHz CPU and 9.0 GB of RAM.

A. Multistate Aircraft Performance

To best show the effects of each geometry on the performance metric, the scatterplots in Fig. 10 were constructed, plotting bank angle vs specific excess power for each state. Each plot contains 23 geometries, with the baseline geometry marked by dashed lines. Note that several geometries may overlap; thus, not all 23 instances are discernible on each plot. The safe region is defined in each plot by a rectangle bounded by the W_M limits of ≥ 200 ft/ min for P_s and within ± 5 deg of the commanded bank angle of 30 deg as defined previously in Sec. IV. Geometries within the safe region are considered operational for the particular failure sequence, whereas those outside of this region will not allow safe completion of the mission. This information is used when classifying the performance of a particular Markov state for the calculation of the expected availability as per Eq. (11).

Of the 184 simulation cases (23 geometries $\times$ 8 states), 28 did not achieve safe performance as established by the W_M criterion on climb rate and bank angle. Twenty-three of these resulted in total loss of aircraft and came from state 7, which was to be expected because there was no way to control the aircraft without use of rudder, aileron, or differential thrust. Four unsatisfactory cases came from the analysis of state 4, where the left engine and ailerons were failed, requiring bank angle and turn to be controlled with only the rudder in the face of asymmetric thrust. The remaining case came from state 5, with the left engine and rudder failed and bank angle controlled with ailerons.

The most critical failing geometries of state 4 were those with the vertical tail height decreased by 10% and the spanwise engine location at the greatest distance from the fuselage. The short tail height was also the failing geometry of state 5. Experimentation with

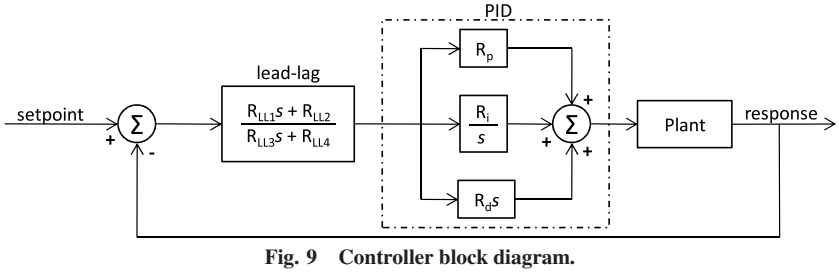

Fig. 9 Controller block diagram.

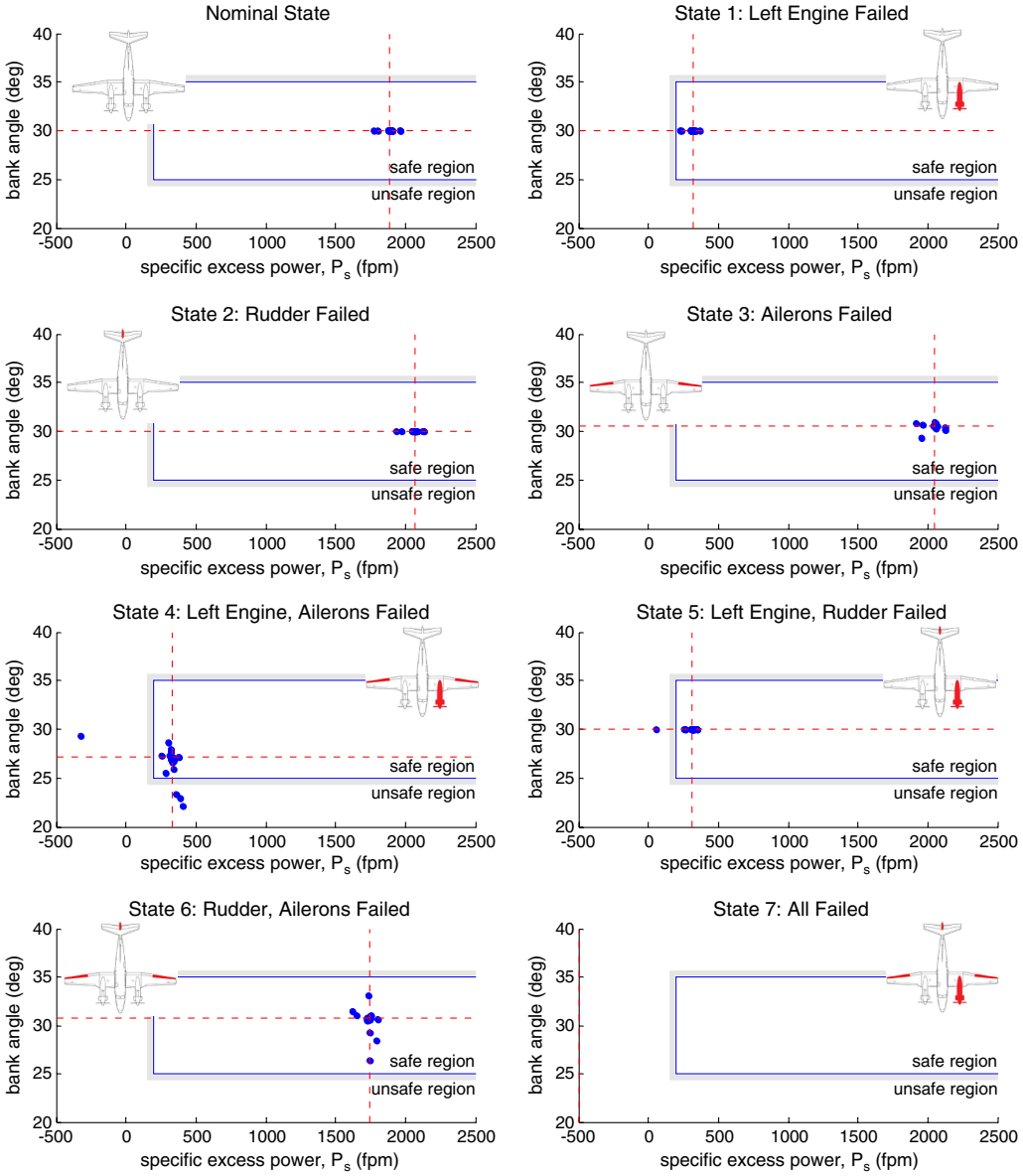

Fig. 10 Effect of geometry perturbation on P_s vs bank angle for each Markov state. States correspond to those in Fig. 8. Inset aircraft diagrams show failed components.

the control scenarios for this state as well as numerous hours of flight testing actual Beech 200 aircraft motivated suspicion that an unsatisfactory Dutch roll mode might be to blame. Indeed, inspection of the control derivatives showed that these two geometries had the lowest values for $|C_{n\beta}/C_{l\beta}|$ of all 23 cases. A general rule in aircraft design is that $|C_{n\beta}/C_{l\beta}|$, which is a measure of the aircraft's lateral stability in relation to its directional stability, should be greater than 0.33 for satisfactory Dutch roll. For the case with the reduced tail height, this value was 0.19 and for the outboard engine placement it was 0.31.

There are a few items to note concerning this finding. First, the design model predicted a $|C_{n\beta}/C_{l\beta}|$ of 0.38 for the baseline aircraft and data collected from the flight testing in March 2010 [39] indicated a value somewhat less than this but within the margin of error. Both of these values are very close to the 0.33 threshold and become more critical at higher AOAs, as less of the tail is in undisturbed flow. This is a known characteristic of the Beech 200 and one of the reasons why the aircraft is equipped with a yaw damper (the yaw damper is only certified for nominal operation and is shut off in failure conditions, per flight manual emergency procedures). Second, in five of the eight states, these poor Dutch roll characteristics did not result in a loss of the aircraft. However, in the adverse circumstances presented by state 4, the rudder was unable to dampen the Dutch roll mode while also being required to control bank angle in a turning climb. Although it may be argued that this particular outcome is specific to the scenario and optimum control laws presented here, it does demonstrate the emergence of critically negative behavior in off-nominal conditions that can be affected by small changes in geometric design variables. Specifically, a slightly more effective vertical tail would have been helpful in supporting both functions; controlling the Dutch roll mode, and maintaining bank angle.

Finally, regarding engine placement, in some cases intuition might be correct in suggesting further outboard engine location is desirable for better turn control through differential thrust. However, results show that the effect of this placement on inertial and mass properties should not be overlooked, especially when certain stability characteristics lie on the margin as in the case of state 4.

B. Sensitivity Analysis

It is important to determine which parameters have the greatest effect on overall system performance and availability. As mentioned earlier, the expected performance in Eq. (6) tends to treat the Markov-state probabilities as weights. Thus, given sufficiently low failure rates, a short Markov time period will have expected performance

Table 5 Steady-state Markov probabilities

Markov state	8 h sortie	20,000 h system lifetime	Five-year sortie
Nominal	99.9%	67.0%	41.6%
State 1	0.01%	25.3%	42.3%
State 2	<0.001%	2.7%	3.8%
State 3	<0.001%	2.7%	3.8%
State 4	<0.001%	1.0%	3.9%
State 5	<0.001%	1.0%	3.9%
State 6	<0.001%	0.1%	0.35%
State 7	<0.001%	0.04%	0.35%

values nearly identical to the nominal state. As overall system lifetime increases, or mission duration in the case of long-endurance vehicles, the expected system performance will change as off-nominal probabilities increase. To illustrate this, consider an 8 h mission and a 20,000 h system lifetime, both typical for this type of aircraft. If no repairs are made, the Markov-state probabilities will be as those depicted in Table 5, given the failure rates mentioned earlier. Even if repairs are considered, these values provide some indication of the amount of resources that must be allocated towards maintenance. The third column in Table 5 is not necessarily applicable to this aircraft, but is included to emphasize the impact of this analysis on systems expected to operate for long periods of time in austere environments, for instance an ultra-long-endurance unmanned vehicle with a continuous mission duration of five years [27].

Given these probabilities, it is possible to determine the expected system performance and availability. More important, one may solve the expected performance sensitivity for the 8 h sortie, 20,000 h system lifetime, or five-year case, or likewise observe changes in expected availability. The design variable sensitivities are simple perturbations from the baseline geometry, figured from a central difference on the high and low variations in Table 4, according to Eq. (14):

$$\frac{\Delta E_{A,G}(\mathbf{x},\boldsymbol{\lambda})}{\Delta \mathbf{x}} = \frac{E_{A,G}(\mathbf{x}+\Delta\mathbf{x},\boldsymbol{\lambda}) - E_{A,G}(\mathbf{x}-\Delta\mathbf{x},\boldsymbol{\lambda})}{2\Delta\mathbf{x}} \tag{14}$$

Similar calculations were made for perturbations to the individual component failure rates (aileron, rudder, and engine), also varied by 10%. These were normalized by the baseline aircraft geometry and expected values. The sensitivities for the 8 and 20,000 h expected P_s are shown in Fig. 11.

The 8 h sortie represents a nominal aircraft sensitivity analysis for specific excess power, as might traditionally be performed in aircraft design. Here, wing span b is the most sensitive component. This is due to the significant increase in wing mass with the increase in aspect ratio, which outweighs the reduction in induced drag that occurs with a larger span. Wing area S is the next highest contributor, again due mostly to changes in the mass of the lifting surface. The sign of this sensitivity is opposite to that with wing span, as would be predicted by the location of S in the denominator of the equation for aspect ratio, $AR = b^2/S$.

Results change for the 20,000 h system lifetime sensitivity. Wing span and area remain two of the three most influential variables; this is to be expected, given that the nominal state still has a 67% probability and thus retains a significant influence. However, previously insensitive variables are now more prominent. These are engine failure rate, vertical tail height, and vertical tail area. The first, engine failure rate, comes as little surprise given the relatively high probability of an engine failure, which is 27.3% per summation of Markov states 1, 4, 5, and 7 in Table 5. Hence, reducing engine failure rate would, naturally, have a beneficial effect on the expected specific excess power. The vertical tail height is less obvious. In this case, the derivative actually changes sign, in addition to magnitude, between the more nominal scenario and the extended time duration scenario that gives more weight to the off-nominal states. This arises from the unsatisfactory performance shown in states 4 and 5, as well as from having nearly the worst performance in state 3. The fact that this geometry performs quite well in the remainder of the states illustrates the importance of observing the design space from a multistate perspective, especially when long time durations are considered.

Figure 12 shows the same type of sensitivity results but for expected bank-angle deviation instead of specific excess power. Again, vertical tail height is an extremely important factor in the 20,000 h scenario, whereas it is relatively benign in the 8 h sortie. In

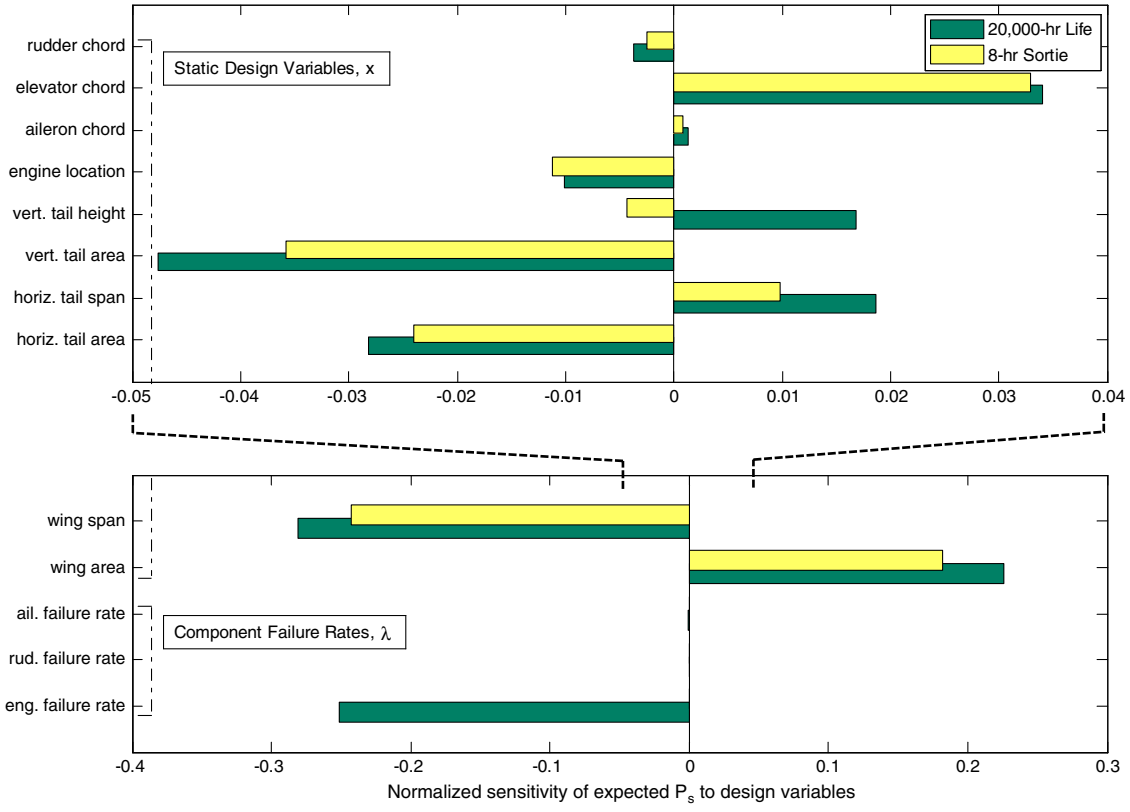

Fig. 11 Comparison of design sensitivities: P_s, sensitivity $= \Delta E_G(P_s)/\Delta x * (x_0/E_{G,0}(P_s))$. Top chart zoomed in for detail.

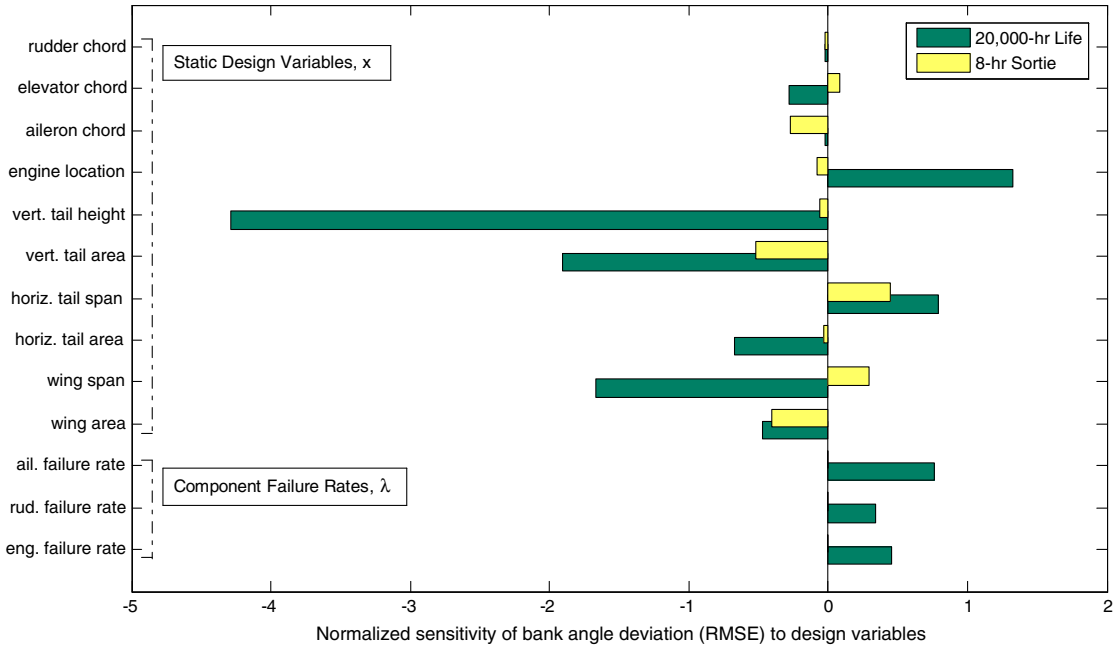

Fig. 12 Comparison of design sensitivities: ϕ_{dev}, sensitivity $= \Delta E_G(\phi_{\text{dev}})/\Delta x * (x_0/E_{G,0}(\phi_{\text{dev}}))$.

addition, several sensitivities such as wing span, engine location, and elevator chord change in both sign and magnitude. Note that sensitivity to engine failure rate is much less significant in comparison to the other failure rates than in Fig. 11. This is due to the fact that a significant portion of bank angle deviation occurs in states 3 and 6, in which the engine has not failed.

Finally, the data in Fig. 13 demonstrate how changes in design variables and component failure rates affect the system expected availability. The driving factors are those pointed out previously in the analysis of the scatterplots in Fig. 10. Although the engine has the highest component failure rate, its effect on expected availability is less than the other two components because the failure rate sensitivities were performed from the baseline geometry, which only has unsatisfactory performance in state 7. The distribution of probabilities across Markov states for this geometry is such that changes to aileron and rudder failure rates actually increase the weighting of state 7 more than do changes to the engine failure rate. Only the 20,000 h and five-year results are shown, as those for the 8 h duration are insignificant in magnitude.

C. Reachability

Special care was taken to ensure that the results of the worst-performing states were not merely due to an inappropriate selection of gains for the specified control system. One means of doing this was careful formulation of the gain optimization given in Eq. (12), examination of the resulting postoptimality criterion, and comparison of results from multiple starting points within the design space, all of which indicated that the best possible solution had been obtained. As a second means of verification, a comparison of system reachability was made between satisfactory and nonsatisfactory geometries, a full discussion of which is provided in Appendix B. Indeed, the results of this analysis indicated a distinct difference, for instance, between the reachability of the low vertical tail height

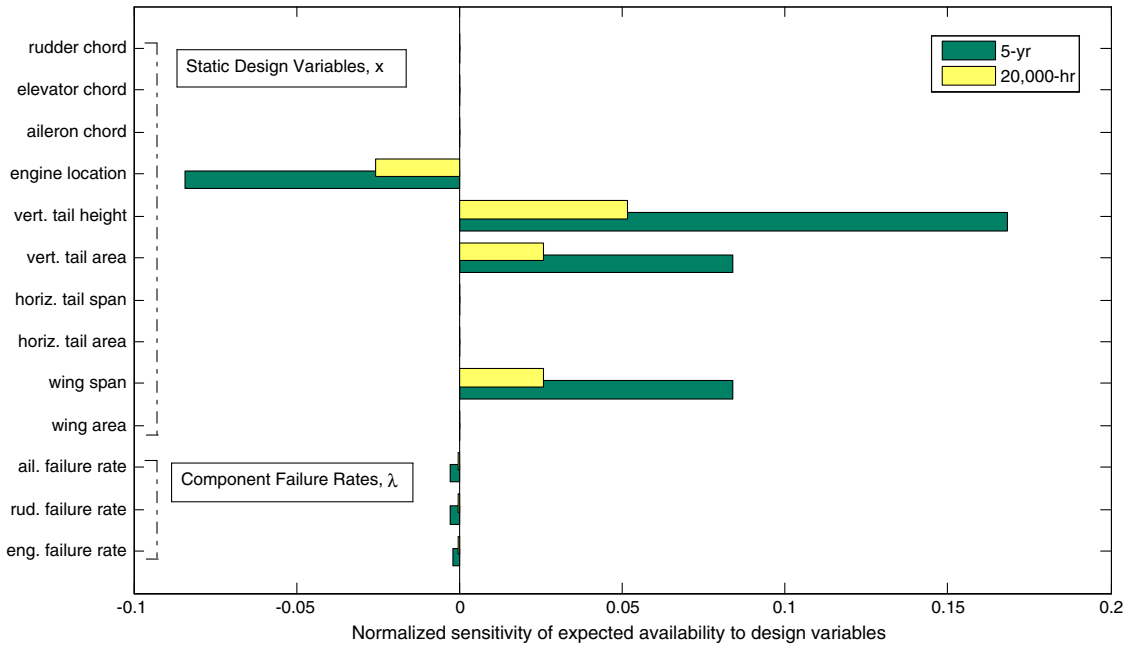

Fig. 13 Comparison of design sensitivities: E_A, sensitivity $= \Delta E_A(P_s, \phi)/\Delta x * (x_0/E_{A,0}(P_s, \phi))$.

geometry system and the baseline geometry system of state 4, namely that the worst-performing system was not reachable, whereas the baseline system was reachable.

VI. Conclusions

In summary, a multistate design approach was introduced that enables the rapid and flexible analysis of multistate aircraft performance. The approach was applied to the case study of an existing twin-engine aircraft. Results showed how small changes in static design variables may improve performance in the nominal condition while hurting performance in off-nominal conditions, resulting in decreased expected performance or availability across system lifetime or long mission durations. Specific results from the Super King Air analysis showed that, of 184 geometry cases, 28 did not achieve satisfactory performance. Many occurred in the fully failed state and were expected, but several occurred in partially degraded states in which the majority of geometry cases were able to meet performance requirements. More important, this behavior clearly exhibited itself in the resulting design sensitivities, confirming that such an approach will allow designers to identify those elements that might drive system loss probability through an analysis of performance changes across system states and their respective response to changes in design variables.

The results of this study provide promising evidence as to the utility of expected performance and expected availability analysis and its ability to provide design engineers with data to generate more robust solutions early in the design process. Future work will expand the expected value sensitivity analysis experiments. Having validated these methods on this well defined aircraft problem, the next step is application to a larger, less understood model, and extension to states with failed sensors or instruments leading to degradation with less than full observability.

Appendix A: Failure Rates

The authors chose to use what are considered typical values of failure rates to illustrate effectiveness of the technique at identifying potential issues with the design's performance under failure, even given low failure rates. Flight-control-system failure rates were conservative estimates often used by experts of $1/500,000$ h. Guidance for these values can be derived from National Transportation and Safety Board (NTSB) data, such as its Annual Review of Accident Data. For example, 2006 data show that Part 135 airplane operations had one accident attributable to flight-control-system failure over 2.5 million hours of operation [42]. Because the Super King Air is generally a Part 135 on-demand or scheduled charter aircraft, and not all flight-control-system failures result in what the NTSB considers an accident, the authors consider a 500,000 h MTBF for the aileron and rudder control system as a reasonable estimate. Failure rates can vary widely across aircraft (for some examples of very poor rates, e.g., $1/5000$ h in UAVs, see [43]), but for purposes of design the direction of performance improvement is typically much more important than the absolute magnitude of expected availability or expected performance resulting from a specific combination of failure rates.

Appendix B: Reachability

The state-space system described by

$$\dot{\mathbf{x}} = A\mathbf{x} + B\mathbf{u} \qquad \mathbf{y} = C\mathbf{x} + D\mathbf{u} \tag{B1}$$

in which $\mathbf{x}(t) \in \mathbb{R}^n$ is the state vector, $\mathbf{u}(t) \in \mathbb{R}^m$ is the input vector, and $\mathbf{y}(t) \in \mathbb{R}^p$ is the output vector, is termed reachable if a control input can be selected to drive the system from any initial state to any final state in time t. The are many techniques available for solving the reachability problem for discrete time, one of which is the formation and analysis of the reachability matrix, which is defined as

$$Q = [B|AB|A^2B|\ldots|A^{n-1}B] \in \mathbb{R}^{n\times nm} \tag{B2}$$

If and only if the matrix Q has full rank n is the system reachable. This characteristic arises from the nature of the system zeros, which may be divided into three categories: input-decoupling zeros, output-decoupling zeros, and transmission zeros. Only the input-decoupling zeros will be discussed here as they are most relevant to the reachability problem, but the reader is directed to [44] for a full treatment of the topic.

The above mentioned zeros for a multiple-input multiple-output system can be derived from the Rosenbrock system matrix, given in the Laplace domain as

$$P(s) = \begin{bmatrix} sI - A & B \\ C & D \end{bmatrix} \tag{B3}$$

The input-decoupling zeros are the values of s where the upper block matrix (describing the input coupling) of Eq. (B3), given below as Eq. (B4),

$$P_u(s) = [sI - A|B] \in \mathbb{R}^{n\times(n+m)} \tag{B4}$$

has rank less than n. This occurs when multiple paths exist to the same system output or alternate physical mechanisms result in competing output components [45]. The existence of input-decoupling zeros means that control effectiveness is unachievable with the given set of inputs. Furthermore, reachability is equivalent to the absence of input-decoupling zeros.

Equations (B2) and (B4) provide a convenient means for verifying the performance of the worst-performing states as reported in Sec. V. As an example, consider the results shown in state 4 of Fig. 10. Here, Eqs. (B2) and (B4) were used to determine the reachability of the baseline geometry system as compared to the low-tail-height geometry system, where the baseline geometry performance fell well within the safe region, whereas the low tail height geometry was the leftmost point outside of it.

The initial step in this process was to construct the state matrix A, the control matrix B, and the output matrix C (the feed-forward matrix D was null). This was accomplished using an interior-point optimization algorithm acting on the state derivatives to trim the aircraft model as close as possible to the desired flight conditions for both geometries. The model was then linearized about these points using an algorithm adapted from Stevens and Lewis [45], to obtain two distinct, geometry-specific sets of (A, B, C). Although only A and B are needed for the evaluation of Eq. (B2), C was used to find the system zeros from Eq. (B3) for the rank evaluation of Eq. (B4). For state 4, the state vector consisted of $[U, V, W, P, Q, R, \phi, \theta, \psi, \text{pos}_N, \text{pos}_E, h]$, while the input vector was $[\delta_{\text{elevator}}, \delta_{\text{rudder}}]$ with output of $[P, R, \phi, \psi]$, recalling that, for this state, the ailerons and left engine were failed.

Results showed a distinct difference in the degree of reachability for the two geometries. The rank of Q from Eq. (B2) for the baseline geometry was 12 (full rank, because $n = 12$), indicating a reachable system. For the low tail geometry, the rank dropped to 11 for the same tolerances, indicating an unreachable system and implying the existence of one or more input-decoupling zeros. Further examination of the system zeros and subsequent evaluation of $P_u(s)$ from Eq. (B4) showed the presence of one input-decoupling zero near the origin for the low tail geometry and confirmed the absence of input-decoupling zeros for the baseline geometry system.

References

[1] Barlow, R. E., and Wu, A. S., "Coherent Systems with Multi-State Components," *Mathematics of Operations Research*, Vol. 3, No. 4, 1978, pp. 275–281. doi:10.1287/moor.3.4.275

[2] Lisnianski, A., and Levitin, G., *Multi-State System Reliability: Assessment, Optimization, and Applications*, Vol. 6, Series on Quality, Reliability and Engineering Statistics, World Scientific, Singapore, 2003, pp. 257–350.

[3] Steinberg, M., "Historical Overview of Research in Reconfigurable Flight Control," *Journal of Aerospace Engineering*, Vol. 219, No. 4, 2005, pp. 263–275.

[4] Burcham, F. W., and Fullerton, C. G., "Controlling Crippled Aircraft—

With Throttles," NASA TM 104238, 1991.
[5] Dornheim, M. A., "Research Pilot Devises Rules of Thumb for Engine-Only Control of Disabled Aircraft," *Aviation Week and Space Technology*, Vol. 134, No. 25, 1991, p. 43.
[6] Barrett, W. J., Rembold, J. P., Burcham, F. W., and Myers, L. P., "Digital Electronic Engine Control System F-15 Flight Test," *Journal of Aircraft*, Vol. 20, No. 2, 1983, pp. 134–141.
[7] Burcham, F. W., Myers, L. P., and Walsh, K. R., "Flight Evaluation of a Digital Electronic Engine Control in an F-15 Airplane," *Journal of Aircraft*, Vol. 22, No. 12, 1985, pp. 1072–1078. doi:10.2514/3.45252
[8] Burcham, F. W., Maine, T. A., Fullerton, C. G., and Webb, L. D., "Development and Flight Evaluation of an Emergency Digital Flight Control System Using Only Engine Thrust on an F-15 Airplane," NASA TP 3627, Sept. 1996.
[9] Ward, D. G., and Monaco, J. F., "System Identification for Retrofit Reconfigurable Control of an F/A-18 Aircraft," *Journal of Aircraft*, Vol. 42, No. 1, 2005, pp. 63–72. doi:10.2514/1.2941
[10] Dugan, J., Bavuso, S., and Boyd, M., "Dynamic Fault Fault-Tree Models for Fault-Tolerant Computer Systems," *IEEE Transactions on Reliability*, Vol. 41, No. 3, 1992, pp. 363–377. doi:10.1109/24.159800
[11] Smotherman, M., and Zemoudeh, K., "A Non-Homogeneous Markov Model for Phased-Mission Reliability Analysis," *IEEE Transactions on Reliability*, Vol. 38, No. 5, Dec. 1989, pp. 585–590. doi:10.1109/24.46486
[12] Rausand, M., and Hoyland, A., *System Reliability Theory*, 2nd ed., Wiley,
Hoboken, NJ, 2004, pp. 96–106, 118–125.
[13] Reibman, A., and Veeraraghavan, M., "Reliability Modeling: An Overview for System Designers," *Computer*, Vol. 24, No. 4, 1991, pp. 49–57.
[14] Babcock, P. S., IV., "Channelization: The Two-Fault Tolerant Attitude Control Function for the Space Station Freedom," *IEEE Aerospace and Electronics Systems Magazine*, Vol. 11, No. 5, 1996, pp. 9–22. doi:10.1109/62.494183
[15] Babcock, P. S., IV., and Zinchuk, J. J., "Fault-Tolerant Design Optimization: Application to an Underwater Vehicle Navigation System," *Proceedings of the 1990 Symposium on Autonomous Underwater Vehicle Technology*, IEEE Publ., Piscataway, NJ, June 1990, pp. 34–43.
[16] Siddiqi, A., de Weck, O., and Iagnemma, K., "Reconfigurability in Planetary Surface Vehicles: Modeling Approaches and Case Study," *Journal of the British Interplanetary Society*, Vol. 59, No. 12, 2006, pp. 450–460.
[17] Haas, P. J., *Stochastic Petri Nets: Modelling, Stability, Simulation*, Springer–Verlag, New York, 2002, pp. 19–24.
[18] Dominguez-Garcia, A. D., Kassakian, J. G., Schindall, J. E., and Zinchuk, J. J., "An Integrated Methodology for the Dynamic Performance and Reliability Evaluation of Fault-Tolerant Systems," *Reliability Engineering and System Safety*, Vol. 93, No. 11, 2008, pp. 1628–1649. doi:10.1016/j.ress.2008.01.007
[19] Babcock, P. S., IV., Rosch, G., and Zinchuk, J. J., "An Automated Environment for Optimizing Fault-Tolerant Systems Designs," *Proceedings of the 1991 Annual Reliability and Maintainability Symposium*, IEEE Publ., Piscataway, NJ, Jan. 1991, pp. 360–367.
[20] Meng, W., and Ma, D., "Robust Design Optimization Method for Aircraft," *Proceedings of the 3rd International Symposium on Systems and Control in Aeronautics and Astronautics*, IEEE Publ., Piscataway, NJ, June 2010, pp. 430–434.
[21] Ghizu, T., Jarrett, J. P., and Parks, G. T., "Robust Design Optimization of Airfoils with Respect to Ice Accretion," *Journal of Aircraft*, Vol. 48, No. 1, 2011, pp. 287–304. doi:10.2514/1.C031100
[22] Huang, B., and Du, X., "Analytical Robustness Assessment for Robust Design," *Structural and Multidisciplinary Optimization*, Vol. 34, No. 2, 2007, pp. 123–137. doi:10.1007/s00158-006-0068-0
[23] Bhat, U. N., and Miller, G. K., *Elements of Applied Stochastic Processes*, Wiley, Hoboken, NJ, 2002, p. 31.
[24] Babcock, P. S., IV., "An Introduction to Reliability Modeling of Fault-Tolerant Systems," Charles Stark Draper Lab. CSDL-R-1899, Cambridge, MA, Sept. 1986.
[25] Levitin, G., and Lisnianski, A., "A New Approach to Solving Problems of Multi-State System Reliability Optimization," *Quality and Reliability Engineering International*, Vol. 17, No. 2, 2001, pp. 93–104. doi:10.1002/qre.388
[26] Borer, N. K., Claypool, I. R., Clark, W. D., West, J. J., Odegard, R. G., Somervill, K. M., et al., "Model-Driven Development of Reliable Avionics Architectures for Lunar Surface Systems," *2010 IEEE Aerospace Conference*, IEEE Publ., Piscataway, NJ, March 2010, pp. 1–21.
[27] "Vulture Program," Defense Advanced Research Projects Agency, Tactical Technology Office, Broad Agency Announcement 07-51, Arlington, VA, July 2007.
[28] Brandt, S. A., Stiles, R. J., Bertin, J. J., and Whitford, R., *Introduction to Aeronautics: A Design Perspective*, 2nd ed., AIAA, Reston, VA, 2004, pp. 345–370.
[29] Raymer, D. P., *Aircraft Design: A Conceptual Approach*, 3rd ed., AIAA, Reston, VA, 1999, pp. 467–480.
[30] Drela, M., and Youngren, H., "Athena Vortex Lattice Solver," Massachusetts Inst. of Technology, http://web.mit.edu/drela/Public/web/avl/ [retrieved March 2010].
[31] Richards, J., Aarons, T., Suleman, A., Caneld, R. A., Woolsey, C., Lindsley, N., et al., "Design for Flight Test of a Scaled Joined Wing SensorCraft," Proceedings of the 52nd AIAA/ASME/ASCE/AHS/ASC Structures, Structural Dynamics and Materials Conference, Denver, CO, AIAA Paper 2011-2011, April 2011.
[32] Leong, H., Jager, R., Keshmiri, S., and Colgrem, R., "Development of a Pilot Training Platform for UAVs Using a 6DOF Nonlinear Model with Flight Test Validation," Proceedings of the 2008 AIAA Modeling and Simulation Technologies Conference and Exhibit, Honolulu, HI, AIAA Paper 2008-6368, Aug. 2008.
[33] Boschetti, P. J., Cardenas, E. M., Amerio, A., and Arevalo, A., "Stability and Performance of a Light Unmanned Airplane in Ground Effect," Proceedings of the 48th AIAA Aerospace Sciences Meeting, Orlando, FL, AIAA Paper 2010-293, Jan. 2010.
[34] Berndt, J., and de Marco, A., "Progress On and Usage of the Open Source Flight Dynamics Model Software Library, JSBSim," Proceedings of the 2009 AIAA Modeling and Simulation Technologies Conference, Chicago, AIAA Paper 2009-5699, Aug. 2009.
[35] Mills, B., "DIY Drones: Prole of Brian Mills," http://diydrones.ning.com/profile/BrianMills [retrieved March 2010].
[36] "Operator's Manual for Army C12-C, D, T Aircraft," U.S. Army TM 1-1510-218-10, Sept. 2001.
[37] "Hawker Beechcraft Model 200 Type Certificate," Federal Aviation Admin. Type Certificate Data Sheet No. A24CE, Rev. 99, 2009.
[38] Thompson, S., and Agte, J., "C-12C Aerodynamic Model Evaluation," U.S. Air Force TR 2001-01A-1, Edwards AFB, CA, April 2001.
[39] Creech, N. A., Burton, T. A., Cuadra, P., Harder, A. D., Odom, R. L., and Wisecup, J. S., "C-12C Parameter Estimation," U.S. Air Force TR 2010-09B-1, Edwards AFB, CA, March 2010.
[40] "The Status of Commercial Passenger Operations in Turbine Powered Single Engine Aeroplanes," Australian Bureau of Air Safety Investigation TR SAB/IP/93/4, Canberra, Australia, Dec. 1993.
[41] Ziegler, J. G., and Nichols, N. B., "Optimum Settings for Automatic Controllers," *Journal of Dynamic Systems, Measurement, and Control*, Vol. 115, No. 2B, 1993, pp. 220–222.
[42] "Annual Review of Aircraft Accident Data—U.S. Air Carrier Operations Calendar Year 2006," National Transportation Safety Board TR NTSB/ARC-10/01, Washington, DC, Dec. 2006.
[43] "Unmanned Aerial Vehicle Reliability Study," Department of Defense Rept., Washington, DC, Feb. 2003, http://www.uadrones.net/military/research/acrobat/0302.pdf [retrieved 11 April 2012.
[44] Antsaklis, P. J., and Michel, A. J., *A Linear Systems Primer*, Birkhauser, Boston, 2007, pp. 195–230.
[45] Stevens, B. L., and Lewis, F. L., *Aircraft Control and Simulation*, 2nd ed., Wiley-Interscience, New York, 2003, pp. 643–653.